Nucleic Acids Research, 2025, **53**, gkaf106
https://doi.org/10.1093/nar/gkaf106
Genome integrity, repair and replication

Phosphorylated BLM peptide acts as an agonist for DNA damage response

Ritu Agrawal[1,2], Himanshi Agarwal[1], Chetana Mukherjee[1], Baishali Chakraborty[1], Vandana Sharma[1], Vivek Tripathi[1,3], Nitin Kumar[1], Swati Priya[1], Nidhi Gupta[4], Gagan Deep Jhingan[5], Avinash Bajaj[4], Sagar Sengupta[1,2,*]

[1]Biotechnology Research and Innovation Council—National Institute of Immunology (BRIC-NII), Aruna Asaf Ali Marg, New Delhi 110067, India
[2]Biotechnology Research and Innovation Council—National Institute of Biomedical Genomics (BRIC-NIBMG), Kalyani, West Bengal 741251, India
[3]Present address: Department of Molecular Genetics and Cancer, NUCSER, NITTE University (DU), Mangalore 575018, Karnataka, India
[4]Regional Centre for Biotechnology, Faridabad 121001, Haryana, India
[5]Valerian Chem Pvt. Ltd, Vproteomics, Green Park, Delhi 110016, India
[*]To whom correspondence should be addressed. Email: ssg2@nibmg.ac.in

Abstract

Upon exposure to ionizing irradiation, the MRE11–RAD50–NBS1 complex potentiates the recruitment of ATM (ataxia-telangiectasia mutated) kinase to the double-strand breaks. We show that the lack of BLM causes a decrease in the autophosphorylation of ATM in mice mammary glands, which have lost one or both copies of BLM. In isogenic human cells, the DNA damage response (DDR) pathway was dampened in the absence of BLM, which negatively affected the recruitment of DDR factors onto the chromatin, thereby indicating a direct role of BLM in augmenting DDR. Mechanistically, this was due to the BLM-dependent dissociation of inactive ATM dimers into active monomers. Fragmentation analysis of BLM followed by kinase assays revealed a 20-mer BLM peptide (91–110 aa), sufficient to enhance ATM-dependent p53 phosphorylation. ATM-mediated phosphorylation of BLM at Thr99 within BLM (91–110) peptide enhanced ATM kinase activity due to its interaction with NBS1 and causing ATM monomerization. Delivery of phosphomimetic T99E counterpart of BLM (91–110 aa) peptide led to ATM activation followed by restoration of the DDR even in the absence of ionizing irradiation (both in cells and in BLM knockout mice), indicating its role as a DDR agonist, which can be potentially used to prevent the initiation of neoplastic transformation.

Graphical abstract

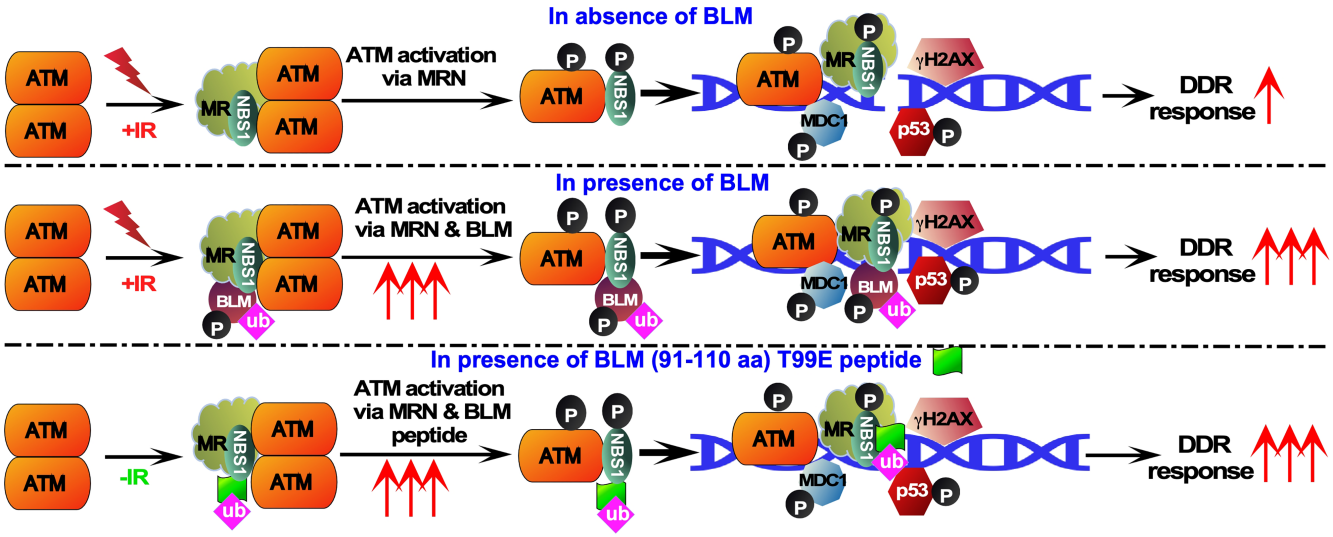

Received: September 18, 2024. **Revised:** January 8, 2025. **Editorial Decision:** January 31, 2025. **Accepted:** February 5, 2025

Introduction

Eukaryotic cells frequently encounter DNA damage from both internal and external sources. To address this, cells have developed sophisticated mechanisms known as the DNA damage response (DDR) signaling pathway. A central player in this pathway is ATM (ataxia-telangiectasia mutated), a serine/threonine protein kinase [1, 2]. When activated, ATM phosphorylates numerous downstream targets such as NBS1, CHK2, p53, and other DDR proteins involved in DNA repair, cell cycle control, autophagy, apoptosis, and senescence [2]. This activation sets off a series of events aimed at either repairing the damaged DNA or triggering cell death if the damage is irreparable, thus safeguarding against the accumulation of mutations and tumorigenesis.

ATM is primarily activated in response to double-strand breaks (DSBs). Upon encountering DNA damage, inactive ATM dimers disassemble into active monomers through their autophosphorylation on Ser1981 [3]. MRE11–RAD50–NBS1 (MRN) complex serves as a sensor for DSBs and plays a crucial role in recruiting ATM to DSB sites, inducing monomerization of the kinase and thereby activating ATM by promoting the interaction of the monomeric ATM with the DNA and substrates [4, 5]. Numerous mechanisms are known to inhibit ATM activity, such as DNA-PKcs-mediated suppression of ATM phosphorylation [6]. Specific ATM inhibitors have been identified that act as ATM antagonists [7]. However, very little is known about the mechanisms that promote and sustain DDR activation.

Both ATM and BLM helicase are integral components of the BRCA1-associated genome surveillance complex (BASC), where they interact and functionally complement each other [8, 9]. Mutations in BLM give rise to a monogenic biallelic Bloom syndrome (BS), a condition associated with heightened susceptibility to various types of cancer [10]. BLM has multiple roles during the process of the development of neoplastic transformation. It plays a crucial role in chromatin remodeling, which leads to chemoresistance [11, 12]. BLM is also involved during DNA damage sensing and DNA repair [13, 14], participating in multiple stages of the homologous repair recombination (HRR) process and has both pro- and anti-recombinogenic functions [15, 16]. BLM also takes part in the initial step of single-stranded DNA (ssDNA) end resection [17], a crucial process in DSB repair. Furthermore, BLM and 53BP1 mutually enhance their accumulation at DSB sites [15, 18–20]. BLM is phosphorylated by both ATM and ATR at Thr99 and Thr122 [9, 21]. BLM is known to be recruited to the sites of stalled replication in both phosphorylation- and ubiquitylation-dependent manner [22, 23]. Importantly, the recruitment of BLM to DSBs relies on ATM kinase activity, Mre11 exonuclease activity, and NBS1, whereas its own helicase activity is dispensable for this recruitment process [24].

In this study, we wanted to determine whether BLM affected ATM activation. We found that the lack of BLM led to a decrease in the autophosphorylation of ATM at serine 1981 [pATM (S1981)] in mice mammary glands that have lost one (BLM HKO) or both copies of BLM (BLM KO). Phosphoproteomic analysis led to the enrichment of pathways that get upregulated when ATM is absent in the mammary glands of BLM HKO and BLM KO mice after exposure to ionizing irradiation (IR). Further usage of multiple experimental models in human cells showed that the loss of BLM not only led to the decrease in pATM (S1981) but also dampened the entire DDR response pathway, consequently negatively affecting the recruitment of these factors onto the chromatin. The presence of BLM led to the dissociation of inactive ATM dimers into active monomers after IR treatment. Biochemically, BLM (91–110 aa) was sufficient to enhance ATM-dependent p53 phosphorylation at serine 15 [p-p53 (S15)]. ATM-mediated phosphorylation of BLM at Thr99 within BLM (91–110) peptide is crucial for enhancing ATM kinase activity via its interaction with NBS1. Both *in vitro* and *in vivo* experiments demonstrated that the usage of phosphorylated BLM (91–110 aa) was capable of ATM activation. These results indicate the presence of a feedforward loop by which phosphorylated BLM Thr99 (91–110 aa) can activate ATM and act as a DDR agonist and thereby sustain DDR response.

Materials and methods

Reagents, antibodies, primers, and recombinants

All antibodies used are listed in Supplementary Table S1. All recombinants used have been described in Supplementary Table S2. All reagents (including chemicals, recombinant proteins, cell lines, peptides, oligonucleotides, animals, deposited data, and other materials) used are described in Supplementary Table S3. All primers are described in Supplementary Table S4.

Biological resources and cell culture

HEK293T, GM03509 GFP Clone 100, GM03509 GFP-BLM Clone 4.3.4, BS3509/A-15, U2OS-AsiSI-ER, and U2OS cell lines were cultured in Dulbecco's modified Eagle's medium supplemented with 10% fetal bovine serum and penicillin–streptomycin solution. Small interfering RNA (siRNA) transfections were carried out by Lipofectamine 2000 according to the manufacturer's protocol for 24–48 h. For western and transcript analysis, 200 pmol of siRNA was transfected using 10 μl of Lipofectamine. Cells were maintained at 37°C and 5% CO_2. BS3509 pLVX IRES, BS3509 pLVX BLM wild-type (1–1417 aa), BS3509 pLVX BLM T99A (1–1417 aa), BS3509 pLVX BLM T99E (1–1417 aa), BS3509 pLVX BLM wild-type (91–110), BS3509 pLVX BLM T99A (91–110), and BS3509 pLVX BLM T99E (91–110) cell lines were selected in 200 μg/ml hygromycin. The U2OS-AsiSI-ER cell line was maintained in 0.5 μg/ml puromycin. HEK293T TLCV2 and HEK293T sgRNA BLM were grown in 2 μg/ml puromycin.

Mice

All animal studies were carried out at the National Institute of Immunology according to approved animal ethics protocols (IAEC/AQ/2015/137, IAEC/AQ/2016/1502, IAEC/AQ/2017/150, IAEC/AQ/2019/182). All mice were housed in pathogen-free environment. BLM mammary tissue-specific knockout has been generated by crossing the *Blm tm4Ches*/J and transgenic MMTV-Cre mice. Mammary tissue-specific BLM wild-type (BLM WT), BLM hetero-knockout (BLM HKO), and BLM knockout (BLM KO) 12-week-old female mice were exposed to 3 Gy IR and sacrificed 1 h post-IR.

CRISPR cell line generation

HEK293T cells were seeded in the 10-cm plate for virus production. At 70%–80% confluency, cotransfection of lentiviral expression plasmids (1:1 ratio), namely TLCV2 BLM

sgRNA 1 for BLM exon 7 (TCACTTGATGGCCCTATGGA) and sgRNA 3 for BLM exon 11 (TAACAGACTCATTTCTACTC) or TLCV2 alone, together with packaging plasmids (pMD2.G, pspax2) was carried out. Transduction was performed in HEK293T cells in 12-well plates using polybrene (10 μg/ml). Medium was changed 16 h post-transduction. Cells were selected with 2 μg/ml puromycin for 14 days.

Lentivirus transduction-based stable cell line generation

HEK293T cells were seeded in 10-cm plates for virus production. At 70%–80% confluency, cotransfection of lentiviral expression plasmids, namely pLVX-IRES-hygro or pLVX-IRES-hygro-BLM wild-type (1–1417 aa), pLVX-IRES-hygro-BLM T99A (1–1417 aa), pLVX-IRES-hygro-BLM T99E (1–1417 aa), pLVX-IRES-hygro-BLM wild-type (91–110), pLVX-IRES-hygro-BLM T99A (91–110), or pLVX-IRES-hygro-BLM T99E (91–110), together with packaging plasmids (pMD2.G, pspax2) (in 1:1:1 plasmid molar ratio) was carried out using Lipofectamine 3000 (in 1:2 ratio). Medium was changed 6 h post-transfection. Viral supernatants were collected 24 and 48 h post-transfection and filtered using a 0.45-μm filter, followed by concentrating the virus overnight using a LentiX concentrator or PEG 8000 (in a 1:3 ratio), followed by centrifugation at 1600 × *g* for 1 h. The viral pellet was dissolved in Tris-EDTA (TE) buffer. Transduction was performed in BS3509 cells in 12-well cluster plates using polybrene (10 μg/ml). Medium was changed 16 h post-transduction. Cells were selected with 200 μg/ml hygromycin for 14 days.

Calcium phosphate transfection

Overexpression of recombinants was performed in HEK293T cells using the calcium phosphate method. For transfection in each well of the six-well cluster plate, the recombinant(s) was added to 0.25 M calcium chloride solution in a transfection tube. The mixture was incubated for 4 min. Subsequently, 2× HEPES buffer of pH 7.2 (280 mM NaCl, 10 mM KCl, 1.5 mM Na_2HPO_4 anhydrous, and 50 mM HEPES) was added dropwise to the transfection tube containing the DNA and $CaCl_2$ mix while vortexing at high speed. The transfection mix was then incubated for 30 min and added dropwise to the cells. Medium was changed 12 h after transfection.

Chromatin fractionation

Cells were grown to a confluency of 70%–80%. Cells were lysed in buffer I (50 mM HEPES, pH 7.5, 150 mM NaCl, 1 mM Ethylenediamine tetraacetic acid (EDTA), 0.05% NP-40, and protease and phosphatase inhibitors) for 5 min on ice. Cell lysate was then centrifuged at 1575 × *g* for 5 min at 4°C. The supernatants were collected in fresh tubes (constituting the soluble fraction). The pellet was washed once with buffer I. It was followed by treating the cells with the extraction with buffer II [50 mM Tris–HCl, pH 7.5, 150 mM NaCl, 1% NP-40, 0.5% sodium deoxycholate, 0.1% sodium dodecyl sulfate (SDS), and protease and phosphatase inhibitors]. The incubation was done on ice for 20 min, after which the extracts were centrifuged at 25,200 × *g* for 20 min at 4°C. The supernatants were collected as the ribonucleoprotein-enriched fraction (constituting the chromatin-bound fraction).

Immunoblotting

For western blotting, cell lysates were prepared using M2 lysis buffer [1 mM Tris–Cl, pH 7.4 or pH 8.0, 150 mM NaCl, 1% Triton X-100, 0.5 mM EDTA, and 0.5 mM Ethylene glycol tetraacetic acid (EGTA) supplemented with 1× Protease Inhibitor Cocktail (PIC)] or RIPA buffer (1 mM Tris–Cl, pH 7.8, 150 mM NaCl, 1% sodium deoxycholate, 0.1% SDS, and 2% Triton X-100 supplemented with 1× PIC). A reducing loading buffer (375 mM Tris–Cl, pH 6.8, 6% SDS, 48% glycerol, 9% β-mercaptoethanol, and bromophenol blue) was added to the lysates (typically 40–60 μg), followed by boiling for 10 min. The samples were run in sodium dodecyl sulfate–polyacrylamide gel electrophoresis (SDS–PAGE) and subjected to immunoblotting with the respective antibodies.

Immunofluorescence

Cells were seeded on the coverslip in the six-well plate. At 60%–70% confluency, cells were fixed with 4% paraformaldehyde for 30 min with mild shaking on ice. Post-fixation, cells were washed twice with 1× phosphate-buffered saline (PBS), after which the cells were permeabilized with 1× PBS containing 0.1% Triton X-100 (PBST). Cells were blocked with 10% normal chicken serum for 1 h. Cells were washed with PBST, followed by incubation with primary antibody for 1 h at room temperature in a humidified chamber, followed by washing and incubation with their respective secondary antibodies for an hour at room temperature. The coverslips were mounted on frosted glass slides with a mounting medium containing 4',6-diamidino-2-phenylindole (DAPI). Cells were visualized and imaged at 63×/1.4 magnification in a Zeiss LSM980 Meta confocal microscope.

For immunofluorescence, mammary gland tissues were excised, washed with 1× PBS, and fixed overnight at room temperature using 10% neutral buffered formalin, pH 6.8 (40% formaldehyde, 45.7 mM NaH_2PO_4, and 33.3 mM Na_2HPO_4). Paraffin-embedded blocks were prepared, and 1–2 μm thick tissue sections were utilized for subsequent staining. Deparaffinization of the tissue sections was carried out using xylene for 25 min, followed by rehydration through sequential immersion in 100%, 90%, and 70% ethanol for 15 min each, concluding with a water wash for 10 min. Antigen retrieval was performed using sodium citrate buffer (10 mM sodium citrate, pH 6.0, and 0.05% Tween 20) in a decloaking chamber (Biocare Medical) for 20 min at 95°C. After cooling at room temperature, the slides were incubated in sodium citrate buffer for 30 min, followed by washing the sections twice with distilled water for 5 min each. Next, endogenous peroxidase activity was blocked with 3% H_2O_2 in methanol for 15 min, after which the sections were washed twice with distilled water for 5 min. Permeabilization and blocking were done simultaneously using 10% goat serum, 0.2% bovine serum albumin (BSA), and 0.4% Triton X-100 in PBS for 60 min at room temperature. Sections were washed for 20 min with 0.4% Triton X-100 and 1% goat serum (washing buffer). The sections were then stained with anti-pATM (S1981) antibody [which also recognizes pATM (S1987) epitope in mice] in a washing buffer overnight at 4°C in a humidified chamber. The next day, sections were subjected to two washes with washing buffer for 10 min each and then stained with an Alexa 488- or Alexa 647-labeled secondary antibody for 2 h. After three additional washes for 10 min each, nuclei were counterstained

with DAPI. All quantitation (immunofluorescence and laser microirradiation) was done by ImageJ.

Protein purification

The GST-tagged p53 or GST-tagged BLM (1–212 aa) proteins were expressed in *Escherichia coli* BL21(DE3) competent cells at 16°C overnight and subsequently purified according to standard protocols by binding to glutathione S-Sepharose. The bound proteins were eluted out using a concentration gradient (1–20 mM) of reduced glutathione. The eluted fractions containing the purified protein were pooled, dialyzed, and used for the assays.

For anti-Flag tag protein purification from mammalian cells, 5 μg of Flag ATM or 4 μg of Rad50, 2.5 μg of NBS1, and 0.4 μg of MRE11 plasmids were cotransfected into HEK293T cells. To purify full-length Flag-tagged BLM and its domain or His-tagged BLM variants (90–110 aa), 3 μg of each plasmid was transfected. One milligram of Flag ATM, full-length Flag BLM, and 500 μg of other lysates were used for immunopurification. Anti-Flag beads (5 μl/IP) for Flag-tagged protein or Ni-NTA beads for His-tagged protein mixed with Sepharose CL-6 beads (30 μl) were incubated with the lysates for 2 h at 4°C. The complexes were washed thrice with the M2 lysis buffer for 5 min. For Flag-tagged protein elution, the protein-bound beads were incubated with Flag peptide (final concentration 100 μg/ml) for 2 h with rigorous tapping every 10-min interval. For the elution of the His-tagged proteins, 200 mM imidazole was used. The centrifugation was done at 2000 rpm for 10 min at 4°C, and the supernatant was collected. Purified eluted proteins were run on the SDS-PAGE, followed by colloidal staining.

In vitro kinase assay

To check ATM kinase activity in the presence or absence of BLM, 1 nM ATM (wild-type or kinase-dead), 9.6 nM MRN, 4 nM BLM, and 10 ng linear ssDNA (∼140 nM) were used to set the kinase assay with 6.25 nM GST-p53. The assay was carried out in a kinase buffer (250 mM HEPES, pH 7.5, 250 mM KCl, 25 mM $MgCl_2$, 25% glycerol, 5 mM ATP, 2.5 mM Dithiothreitol (DTT), 5 mM β-glycerophosphate, and 5 mM sodium orthovanadate) for 90 min at 30°C in a 40 μl reaction. Samples were run on SDS–PAGE, followed by immunoblotting. In parallel, an equivalent amount of GST-p53 was used for the Coomassie staining.

Dimerization assay

For the dimerization assay, Flag-tagged ATM (12 μg) and HA-tagged ATM (24 μg) were cotransfected in a 10-cm plate using calcium phosphate transfection in HEK293T TLCV2 and HEK293T TLCV2 sgRNA BLM cell lines. After 36 h, cells were irradiated with 3 Gy IR, and allowed to recover for 1 h before lysate preparation with M2 lysis buffer (pH 8.0). One milligram of each lysate was used for Flag pull-down, and the immunoprecipitate was used for western blot analysis.

Genotyping

Genomic DNA was isolated from the tail and mammary glands of BLM wild-type, BLM HKO, and BLM KO mice. Polymerase chain reaction (PCR) was performed to amplify the region surrounding exon 7. The touchdown PCR conditions used on tail DNA are as follows: initial denaturation at 94°C for 2 min, (i) denaturation at 94°C for 20 s, (ii) annealing at 65°C for 15 s, which was gradually reduced by 0.5°C per cycle, followed by (iii) extension at 68°C for 10 s. Steps (i)–(iii) were repeated for 10 cycles. This was followed by denaturation at (iv) 94°C for 15 s, (v) annealing at 60°C for 15 s, and (vi) extension at 72°C for 10 s. Steps (iv)–(vi) were repeated for 29 cycles. A final extension step at 72°C for 2 min was performed. The PCR conditions used for LongAmp PCR using mammary tissues are as follows: initial denaturation at 94°C for 30 s, followed by 30 cycles of denaturation at 94°C for 30 s and annealing at 60°C for 3.5 min. The final extension was at 65°C for 10 min. The upper band (1.9 kb) denotes the presence of the *BLM* WT allele, whereas the lower band of ∼500 bp reflects the deletion of the *BLM* exon 7 sequence leading to the generation of either HKOs or KOs.

Phosphoproteomic analysis

BLM WT, BLM HKO, and BLM KO 12-week-old female mice were exposed to 3 Gy IR and sacrificed 1 h post-IR. Mammary glands were isolated and washed using 1× Tris-buffered saline (TBS) with 50 mM NaCl. Protein extraction was carried out by pulverizing the tissue in liquid nitrogen. A solution of 5% SDS and 0.1 M Tris HCl (pH 8.8) buffer was added to the tissue powder. This was followed by sonication with 30-s pulses on/off for 10 cycles on ice. After sonication, the samples were centrifuged at 13,000 rpm for 15 min, and the resulting supernatant was collected. Two milligrams of extracted protein samples were processed using filter-assisted sample preparation methodology, followed by reduction and alkylation with 5 mM tris(2-carboxyethyl)phosphine hydrochloride and 50 mM iodoacetamide and then digested with trypsin (1:50, trypsin/lysate ratio) for 16 h at 37°C. One milligram of dried peptide pellet was dissolved in phthalic acid buffer (0.1% phthalic acid, 2.5% Trifluoroacetic acid (TFA), 20% water, 80% acetonitrile), followed by the addition of TiO_2 beads (Titansphere 5 mm, GL Sciences) and mixed for 2 h on a rotator. The beads were washed twice with phthalic acid buffer, followed by 80% acetonitrile and 0.1% TFA. Bound phosphopeptides were eluted with 0.3 M Ammonium hydroxide (NH_4OH) and the pH was adjusted to around 2 with 50% TFA. Finally, the enriched phosphopeptides were dried using a speed vac and further clarification was performed using C18 mini-columns.

Mass spectrometric analysis of peptide mixtures

The phosphopeptide-enriched dried pellet was resuspended in buffer A (2% acetonitrile, 0.1% formic acid). All mass spectrometric (MS) experiments were performed using an Easy-nLC-1000 system (Thermo Fisher Scientific) coupled to an Orbitrap Exploris 240 mass spectrometer (Thermo Fisher Scientific) equipped with a nanoelectrospray ion source. One microgram of the enriched phosphopeptide mixture was loaded with buffer A and resolved on an Easy-spray column (2 μm resin, 50 cm length) and separated with a 0%–40% gradient of buffer B (80% acetonitrile, 0.1% formic acid) at a flow rate of 300 nl/min and injected for MS analysis. Liquid chromatography gradients were run for 110 min. MS spectra were acquired in the Orbitrap Exploris 240 under the following conditions: maximum ion injection time = 60 ms; AGC target = 300%; RF lens = 70% at a resolution of 60 000 for a mass range of 375–1500. The peptides were dissociated using higher energy collisional dissociation for MS/MS at a colli-

sion energy of 28%. MS/MS spectra were acquired under the following conditions: maximum ion injection time = 60 ms; AGC target = 100% at a resolution of 15 000. MS/MS data were acquired using a data-dependent top 20 method dynamically choosing the most abundant precursor ions from the survey scan, with dynamic exclusion set at 30 s. For internal recalibration during the run, the lock mass option was enabled for polydimethylcyclosiloxane ions ($m/z = 445.120025$).

MS data processing and statistical analysis

All the RAW files were analyzed using Proteome Discoverer v2.5 against the UniProt *Mus musculus* database. For Sequest HT and MS Amanda 2.0 search, the precursor and fragment mass tolerance were set at 10 ppm and 0.02 Da, respectively. The protease was used to generate peptides; i.e. enzyme specificity was set for trypsin/P (cleavage at the C terminus of "K/R: unless followed by "P") along with maximum missed cleavage value of 2. Carbamidomethylation on cysteine was considered as static modification, while oxidation of methionine, acetylation at N-terminus, and phosphorylation at tyrosine, threonine, and serine were considered as dynamic modifications for database search. Both protein false discovery rate and peptide spectrum match (PSM) were set to 0.01 and determined using a percolator node. Relative protein quantification of the proteins was performed using the Minora feature detector node of Proteome Discoverer v2.5 under default settings considering only high PSM confidence.

Chromatin immunoprecipitation

Chromatin immunoprecipitation (ChIP) assays using anti-pATM (S1981) and anti-NBS1 antibodies were carried out in U2OS-AsiSi-ER cells. For this purpose, 250 μl of formaldehyde cross-linked chromatin was immunoprecipitated using 2 μg of the respective antibodies in all the ChIP assays. After washing, the immunoprecipitated complexes were resuspended and cross-linking reversed overnight. DNA was purified by phenol/chloroform, precipitated, and analyzed by ChIP-qPCR. The extent of recruitment of the proteins at the AsiSI-generated cleavage sites was determined by ChIP-qPCR according to the percent input method.

Laser microirradiation

U2OS cells were cultured in a two-well or four-well LabTek chamber (Nunc). The culture dishes were mounted on the stage of the microscope [Axiovert 200 microscope, Palm microlaser workstation (P.A.L.M. Laser Technologies, Germany)]. The incubation was carried out at 5% CO_2 and 37°C. A pulsed nitrogen laser (30 Hz, 337 nm) coupled to the epifluorescence path of the microscope was focused through a C-apochromat 63×/1.2 W Korr UV–VIS water immersion Zeiss objective. The operation was assisted by the PALM Robo-Software. The laser output was set to 35% to generate localized and tractable subnuclear DNA damage. The speed of laser cutting was set to 1. The cells were fixed after 60, 120, and 180 s of irradiation. The cells were then stained using antibodies of interest. DAPI was used to stain the nucleus. Imaging was carried out at 63×/1.4 oil by confocal microscope (LSM 510 Meta, Zeiss). Quantitation of the laser stripe was carried out using Axiovision software (Zeiss). The mean intensity of the stained region of the laser stripe was normalized with an unirradiated region in an unirradiated cell. A graph depicting mean intensity versus time was plotted.

RT-qPCR

Total RNA was isolated from mammary tissue using TRIzol reagent containing 1% β-mercaptoethanol by crushing the tissues in liquid nitrogen. Complementary DNA was generated using a reverse transcriptase core kit according to the manufacturer's protocol. Quantitative PCR (qPCR) reactions were carried out in QuantStudio 3 real-time PCR system.

Southern blot

Genomic DNA was isolated from mouse mammary tissue. Fifteen micrograms of the genomic DNA was digested with HindIII overnight. The resulting fragments were separated by electrophoresis on a 0.8% agarose gel at low voltage (30–40 V) for 6 h. Following electrophoresis, the agarose gel was washed twice with denaturation buffer (0.5 M NaOH, 1.5 M NaCl) for 25 min each, followed by a rinse with deionized water for 10 min, and then with neutralization buffer (1 M Tris, pH 7.5, 1.5 M NaCl) twice for 15 min each. DNA was then transferred to a nylon membrane using capillary action overnight, followed by UV cross-linking. [γ-^{32}P]ATP-labeled probes were prepared using the Random Primers DNA Labeling System (Thermo Fisher Scientific) as per the manufacturer's instructions. After transfer, the membrane was prehybridized in a hybridization buffer at 68°C for 5 min. Prior to probe hybridization, the labeled probe was denatured at 100°C for 10 min and then immediately placed on ice. The denatured probe was added to the prehybridized membrane in its buffer, and the hybridization was allowed to proceed for 10 h at 37°C. After hybridization, the membrane was washed successively with 2× SSC (20× SSC buffer composition: 3 M NaCl, 0.3 M sodium citrate, pH 7) and 0.1% SDS buffer for 5 min, followed by two washes with 0.5× SSC and 0.1% SDS buffer for 20 min each, and finally a wash with 0.1× SSC and 0.1% SDS for 20 min. The membrane was then dried and exposed to a phosphoimager overnight. The phosphoimager screen was scanned using a Typhoon™ laser scanner platform (Cytiva). A 421-bp probe corresponding to BLM exon 8 was used. The hybridization led to the following signal pattern: the 3.9-kb band indicated the presence of floxed BLM allele and the 3.6-kb band indicated the presence of WT BLM allele, while the 2.2-kb band indicated the presence of an allele with exon 7 deletion, i.e. BLM KO allele.

Sucrose density gradient centrifugation

For density gradient centrifugation analysis, cell lysates were prepared in a Tris buffer (pH 8) containing 2× PIC. Six hundred to eight hundred micrograms of lysates (in 200 μl total volume) were layered onto a 10%–30% sucrose gradient containing 1 mM Tris–Cl (pH 7.4) and 150 mM NaCl and centrifuged at 35 000 rpm for 16 h at 4°C using a SW41 rotor (Beckman). Fifteen fractions (0.7 μl each) were collected from the top of the gradient. To each fraction, 100% trichloroacetic acid was added at a 1:10 ratio to induce protein precipitation, and the samples were incubated overnight at −20°C. Following incubation, the samples were centrifuged at 13 000 rpm for 30 min, and the resulting pellets were washed in ice-cold acetone, centrifuged, air-dried, and dissolved in 6× SDS loading dye. The samples were then boiled for 10 min and processed for western blot analysis to identify the fractions containing ATM.

Hydrogel preparations of BLM peptide (91–110 aa)

For animal experiments, hydrogel-based localized delivery of BLM (91–110 aa) T99E or T99A peptide was used. BLM peptide T99E or T99A entrapped gel using a lithocholic acid-derived hydrogelator [25]. Typically, 70 mg of gelator in 1 ml autoclaved water was heated to form a clear solution. For hydrogels, 1.5 mg of peptide was added to the heated solution. The solution was then aspirated in a 1-ml syringe and allowed to cool at room temperature to form a hydrogel, and 0.2 ml of hydrogel was injected orthotopically into the mouse mammary fat pad.

In vitro ATM monomerization assay

Bio-Flag-ATM/HA-ATM dimeric complex was purified by cotransfecting Bio-Flag-ATM (12.5 μg) and HA-ATM (25 μg) in asynchronously growing HEK293T cells. The lysates were subjected to sequential pull-down. First, HA-ATM was pulled down using HA beads and eluted with 1 mg/ml of HA peptide, and then Bio-Flag was pulled down using 30 μl of Dynabeads magnetic streptavidin beads. Fifty nanomolar bead-bound Bio-Flag-ATM/HA-ATM dimeric complex was incubated with 10 nM MRN complex and 100 nM BLM (91–110 aa) peptides (scramble, wild-type, T99A, or T99E) at room temperature for 30 min. Post-incubation, biotinylated protein/complex was separated using a magnet and supernatant was collected. Beads were washed with a buffer containing 100 nM NaCl, 1 mg/ml BSA, and 0.1% CHAPS reagent. Both the beads and the supernatant were resuspended in 6× SDS loading dye, boiled for 10 min, and loaded on 8% denaturing SDS gel [26].

In vitro ubiquitylation assays

The method was adapted from [22]. Ubiquitylation assays were performed using *in vitro* translated full-length BLM and its variants. Assays were set up at 37°C for 3 h. 0.2 μM recombinant His-RNF8 was added to 0.2 μM of the E2 enzyme Ubc13, 0.0125 μM E1, and 8 μM ubiquitin. Reactions were run on 8% SDS–PAGE gel, transferred onto a nitrocellulose membrane, and probed with the indicated antibodies.

Strand annealing assay

Strand annealing reactions were carried out using 1 nM of a ^{32}P-labeled 50-nucleotide oligo (#1) and 1 nM of an unlabeled complementary oligo (#2) [27]. The reactions were prepared in a final volume of 20 μl containing 25 mM Tris–HCl (pH 7.5), 50 mM NaCl, 1 mM EDTA, 10 mg/ml BSA, and 1 mM DTT. Reaction was set up on ice, followed by incubation at 37°C for 5 min. To terminate the reactions, a final concentration of 50 mM EDTA, 1% SDS, 1 mg/ml proteinase K, and 100 nM of the unlabeled version of oligo #1 were added, and the reaction was incubated at 37°C for 15 min. After adding the loading dye, the samples were resolved on a 12% native PAGE gel at room temperature.

Statistical analysis

All measurements are presented as mean ± standard deviation (SD). GraphPad Prism software was employed for statistical analysis. Details about the statistical test used for each experiment have been elaborated in Supplementary Table S5. The specific *P*-values have been indicated.

Results

BLM promotes activation of ATM in response to DSBs

It has been demonstrated that apart from its role in HRR, BLM is also involved in the DDR pathway [13]. Evidence also exists that BLM is involved in sensing both the stalled replication forks [22] and DSBs [28]. In fact, using a kinetic ChIP-qPCR analysis, we have recently demonstrated that BLM is recruited to the vicinity of the DSBs within 30 min of the development of the lesion [28]. Hence, in trying to understand more deeply the role of BLM vis-à-vis DSB-mediated DDR, we created a conditional BLM KO mouse using the MMTV-Cre promoter whereby BLM is deleted in multiple proliferating tissues, including the secretary epithelium of the mammary glands. We verified the tissue-specific knockout of BLM in the mouse mammary glands using genomic DNA PCR (Supplementary Fig. S1A) and Southern blot (Supplementary Fig. S1B). Further BLM transcripts were shown to be downregulated two-fold in BLM heterozygous knockout (BLM HKO) and five-fold in BLM homozygous knockout (BLM KO) mice as compared to BLM wild-type (BLM WT) mice (Supplementary Fig. S1C).

DDR is characterized by large-scale changes in post-translational modifications (including phosphorylation–dephosphorylation cascades) of the sensors, mediators, and effectors that form part of this dynamic yet transient process [29, 30]. Hence, to understand in more detail whether and, if so, how the lack of BLM in the mouse mammary glands affected the global phosphorylation cascade, quantitative phosphoproteomics by MS was performed on the mammary glands obtained from BLM WT, BLM HKO, and BLM KO female mice 1 h after the animals were exposed to 3 Gy IR. Correlation analysis based on the prevalence of unique peptides (Fig. 1A) revealed that the BLM HKO and BLM KO mice were closely aligned with one another compared to BLM WT mice (Fig. 1B). This led to a marked reduction in the phosphopeptide enrichment of *Z*-score <0.5 of ATM substrates (the major kinase regulating the DDR after DSB generation) in BLM KO mice (Fig. 1C).

With an aim to understand the DDR pathways that are deregulated by the absence of BLM, pathway analysis was performed using the unique peptides in BLM WT mice using the WikiPathway database [31]. Multiple pathways associated with ATM activation upon DSBs (like ATM signaling pathway WP2516, ATM signaling network in development and disease WP3878) were upregulated in the BLM WT samples (Fig. 1D). Reciprocally, when kinase perturbation pathway analysis using the GEO database [32] was performed, the ATM knockdown GDS152 pathway was enriched in BLM HKO mice (Fig. 1E). Furthermore, ATM knockout GSE23116 and CHEK2 knockdown GSE27869 pathways were upregulated in BLM KO mice (Fig. 1F), thereby revealing that ATM activation during DDR response due to IR was altered in the absence of BLM.

To confirm the BLM-dependent activation of ATM, immunofluorescence with an anti-pATM antibody was carried out with mouse mammary tissues obtained from mice that have been either exposed or not exposed to IR. Autophosphorylation of ATM was observed in an IR-dependent manner in tissues from BLM WT mice, which was found to be decreased by ∼1.6-fold and ∼3-fold, respectively, in BLM HKO

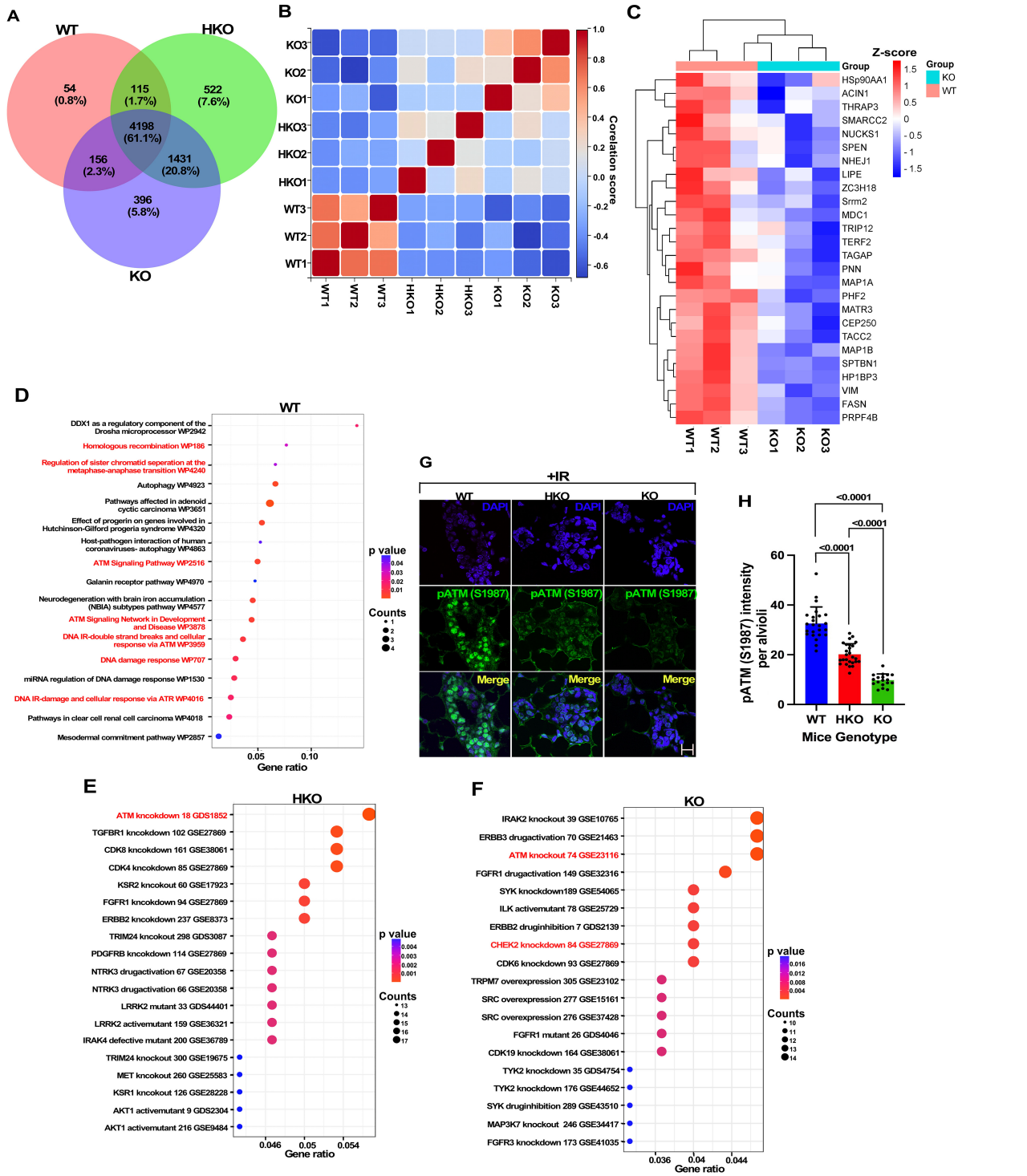

Figure 1. ATM activation is attenuated in BLM KO mice. (**A**) Phosphopeptide enrichment observed in IR-exposed BLM WT, HKO, and KO mice mammary tissues. Female mice aged 12 weeks were subjected to 3 Gy IR. One hour post-IR, the mice were sacrificed, and the mammary glands were isolated and processed for quantitative phosphoproteomics. Venn diagram shows the total and unique phosphopeptides enriched in each genotype of mice ($n = 3$). (**B**) Phosphopeptide enrichment correlation plot shows similarity between BLM KO and HKO mice. Based on the data in panel (A), a correlation plot was generated based on the Pearson score of the phosphopeptides that were enriched in each genotype of mice ($n = 3$). (**C**) Heatmap indicates the downregulation of phosphorylated ATM substrates in BLM KO mice. A heatmap was generated for the relative enrichment of ATM substrates in three genotypes of mice using the phosphopeptide analysis data generated in panel (A). (D–F) Pathway analysis indicates key ATM-mediated pathways are deregulated depending on BLM dosage after IR exposure. Pathway analysis of phosphopeptides enriched in (**D**) BLM WT mice, (**E**) BLM HKO, and (**F**) BLM KO (based on data in panel A) was performed using the WikiPathway (for panel D) and GEO (for panels E and F) databases. (G, H) Levels of phosphorylated ATM reduce in BLM KO mice. BLM WT, HKO, and KO female mice aged 12 weeks were subjected to 3 Gy IR. One hour post-irradiation, the mice were sacrificed, and the mammary tissues were excised. (**G**) Immunofluorescence was carried out using anti-pATM (S1981) antibody that recognizes pATM (S1987). The nuclei were stained with DAPI. Images depict a typical alveolus. Bar: 5 μM. (**H**) Quantitation of the intensity of pATM (S1987) per alveolus of mammary tissue (mean ± SD). Number of tissues analyzed (WT = 24, HKO = 26, KO = 18) was obtained from four mice.

and BLM KO mice tissues (Fig. 1G and H, and Supplementary Fig. S1D and E).

IR-dependent DDR response is an intricately choreographed multistep process in which ATM plays a pivotal role [33]. Hence, we wanted to determine whether BLM-dependent enhanced activation of ATM in mice mammary tissues can be extrapolated to other experimental systems in ±BLM conditions. For different assays, we used multiple pairs of BS patient-derived BLM isogenic lines—GFP-BLM Clone 4.3.4/GFP-100, BS3509 Vector/BLM WT, HEK293T TLCV2/HEK293T TLCV2 sgRNA BLM, and BS 3509/A15. After IR, the presence of BLM enhanced the formation of pATM (S1981) foci by 2.8-fold, p53BP1 (S25/S29) foci by 2.4-fold, and pMDC1 (T4) foci by 4.3-fold (Fig. 2A and B, and Supplementary Fig. S2). The presence of BLM also enhanced the recruitment of phosphorylated ATM by 2.9-fold, MDC1 by 2.6-fold, and NBS1 by 1.6-fold onto the chromatin fraction in two isogenic pairs (Fig. 2C and Supplementary Fig. S3A). BLM-dependent enhanced recruitment of the phosphorylated DDR factors on the chromatin was also seen in U2OS-ASiSI-ER cells in which the DSB has been induced by 4-OHT treatment. Both phosphorylated ATM (by 1.4-fold) and phosphorylated NBS1 (by 1.5-fold) were recruited to a greater extent onto the chromatin within 30 min in cells expressing BLM. A greater amount of pATM (S1981) (by 2.4-fold) was retained on the chromatin even 4 h after DSB induction (Fig. 2D and Supplementary Fig. S3B). To elucidate whether pATM (S1981) was recruited to annotated DSBs, which were generated upon 4-OHT treatment, we carried out ChIP with anti-pATM (S1981) antibody in U2OS-AsiSI-ER cells treated with 4-OHT for 30 min. pATM (S1981) was recruited to both proximal and distal regions to the DSBs on multiple chromosomes only after 4-OHT treatment. Interestingly, the levels of recruitment of pATM (S1981) were reduced by an average of 2.2-fold in cells lacking BLM (Fig. 2E). To determine the dynamics of how BLM enhances the recruitment of the DDR factors, laser microirradiation was performed in U2OS cells in which BLM was depleted by siRNA (Supplementary Fig. S3C). It was observed that the recruitment of both pATM (S1981) and γH2AX at the DNA damage sites was less in the absence of BLM (by ∼2.4–3.6-fold) in a time-dependent manner (Fig. 2F–H).

BLM enhances the formation of ATM monomers

MRN complex is known to activate ATM by multiple mechanisms. While MRN helps in the formation of ATM monomer, it is also phosphorylated by ATM, thereby perpetuating a feed-forward loop [34]. We wanted to determine whether the presence of BLM affects the recruitment of phosphorylated NBS1 onto the chromatin. Laser microirradiation performed on cells in ±BLM conditions revealed that the recruitment of pNBS1 (S343) at the DNA damage sites was reduced in the absence of BLM by ∼1.6–1.8-fold (Fig. 3A and B).

Mediator protein MDC1 amplifies ATM-dependent DDR signals [35]. This occurs due to the phosphorylation-dependent interaction between the MRN complex and MDC1, which allows the retention of MRN on the damaged chromatin [36–38]. We wanted to determine whether BLM, like MDC1, may act like a mediator protein, thereby activating ATM by recruiting the MRN complex. Hence, in U2OS-ASiSI-ER cells, we determined the recruitment of NBS1 to annotated DSBs by ChIP-qPCR. NBS1 recruitment to the tested DSBs was reduced when either BLM or MDC1 was depleted (by ∼2.8–3.0-fold). However, in cells lacking MDC1, exogenously expressed BLM was able to rescue NBS1 recruitment to ∼65%–80% for all tested sites when compared to siControl (Fig. 3C). Together, these results indicate that optimal NBS1 localization to the damaged chromatin involves BLM.

Next, we want to elucidate whether BLM affects ATM activation by enhancing the formation of ATM monomers upon induction of DSBs. For this purpose, Flag-ATM and HA-ATM were cotransfected in HEK293T TLCV2 and HEK293T TLCV2 sgRNA BLM cells, either grown asynchronously or exposed to 3 Gy IR. Lysates were prepared 1 h post-irradiation. Immunoprecipitation using an anti-Flag antibody demonstrated that, following IR, the interaction between Flag-ATM and HA-ATM increased by 1.5-fold in the absence of BLM (Fig. 3D).

Further, to assess the ability of BLM to potentiate the formation of ATM monomers, lysates from IR-exposed GFP-BLM Clone 4.3.4/GFP-100, as well as a newly generated isogenic pair HEK293T TLCV2/HEK293T TLCV2 sgRNA BLM cells, were separated using sucrose density gradient centrifugation followed by the analysis of the gradient fractions to detect ATM distribution. In cells expressing BLM (i.e. in GFP-BLM Clone 4.3.4 and HEK293T TLCV2), ATM was predominantly found in lower sucrose gradient fractions (starting from fraction 9), indicative of the presence of monomeric ATM. Conversely, in cells lacking BLM (GFP100 and HEK293T TLCV2 sgRNA BLM), ATM was detected in higher sucrose gradient fractions (spanning fractions 11–15), thereby indicating the presence of dimeric ATM (Fig. 3E).

Phosphorylated BLM (91–110) enhances ATM kinase activity

In an effort to understand in more detail how BLM can enhance ATM kinase activity, *in vitro* kinase assays were carried out with immunopurified Flag ATM (both wild-type and kinase-dead from cells not exposed to IR), Flag MRN complex (from cells not exposed to IR), Flag BLM (wild-type and its various mutants from cells in ±IR conditions), GST p53 (Supplementary Fig. S4A and B), and sheared double-strand DNA [26]. *In vitro*, kinase assays using a range of wild-type Flag ATM indicated that a minimum of 1 nM of the kinase could phosphorylate GST p53 at serine 15 (Supplementary Fig. S4C). Since BLM seems to enhance DDR response via activating ATM, we wanted to determine whether BLM can enhance p53 phosphorylation. Indeed, immunopurified Flag BLM (only from cells exposed to IR) enhanced the kinase activity mediated by wild-type ATM by ∼2.2-fold, but not by kinase-dead ATM (Fig. 4A and B, and Supplementary Fig. S4D). The presence of MRN was obligatory for the ability of BLM to enhance ATM-mediated phosphorylation (Supplementary Fig. S4E).

In an effort to determine which region of BLM enhanced ATM-mediated phosphorylation on p53, the ATM-mediated kinase assays were repeated in the presence of different BLM fragments (Supplementary Fig. S4B). BLM fragments (1–635 aa) and subsequently (1–220 aa) enhanced ATM-mediated p53 phosphorylation by 2.2- and 3.1-fold, respectively (Supplementary Fig. S5A and B). Subsequently, the usage of smaller deletion fragments and internal deletion of BLM indicated that the minimal region required for

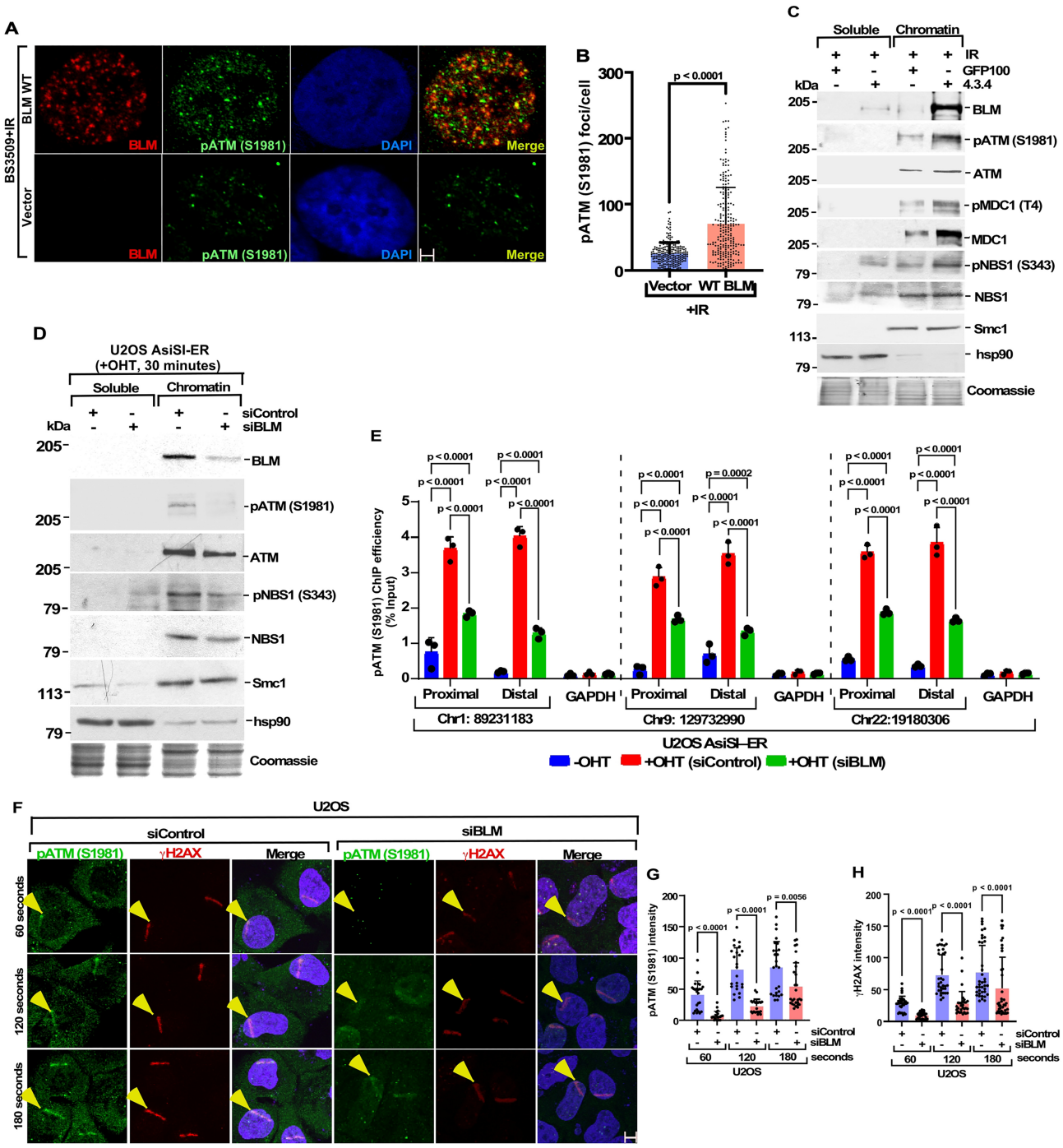

Figure 2. DDR activation is dependent on the BLM upon induction of DSB. (A, B) Formation of ATM foci is enhanced in the presence of BLM after IR exposure. BS3509 vector/WT BLM cells were subjected to IR. Six hours post-IR, the cells were fixed, and (**A**) immunofluorescence was carried out with antibodies against BLM and pATM (S1981). DNA was stained by DAPI. Representative images are shown. Bar: 2 μM. (**B**) Quantitation of the foci in panel (A). Number of nuclei analyzed in each case ($n \geq 150$) from three independent experiments (mean ± SD). (C, D) BLM helicase facilitates optimal loading of DDR factors onto the chromatin in response to DSBs. (**C**) GFP-BLM clone 4.3.4/GFP-100 cells were exposed to IR or (**D**) U2OS-AsiSI-ER cells were exposed to 4-OHT treatment. Soluble and chromatin fractionations were carried out from cells (C) 1 h post-IR or (D) 30 min post-4-OHT treatment. Western blots were carried with antibodies against the indicated antibodies. Coomassie gel shows equal loading of soluble and chromatin-bound fractions. The experiment was done three times. (**E**) Absence of BLM leads to a decrease in pATM recruitment at AsiSI-induced DSBs. U2OS-AsiSI-ER cells were transfected with either siControl or siBLM siRNA. Forty-eight hours post-transfection, the cells were either left untreated or treated with 4-OHT for 30 min. ChIP was carried out using an anti-pATM (S1981) antibody. pATM recruitment to three AsiSI-induced DSBs or GAPDH loci was determined by ChIP-qPCR. Data are from three independent experiments (mean ± SD). (F–H) BLM regulates the early recruitment of pATM and γH2AX at laser microirradiation stripes. Laser microirradiation was performed on U2OS cells after transfecting them with either siControl or siBLM. Cells were fixed 60, 120, and 180 s post-laser microirradiation. (**F**) Immunostaining was carried out using anti-pATM (S1981) and γH2AX antibodies. The nuclei were stained with DAPI. Bar: 2 μM. (G, H) Quantitation of panel (F). (**G**) Quantitation of pATM (S1981). (**H**) Quantitation of γH2AX staining. Quantitation was done from 21 stripes obtained from three independent experiments (mean ± SD).

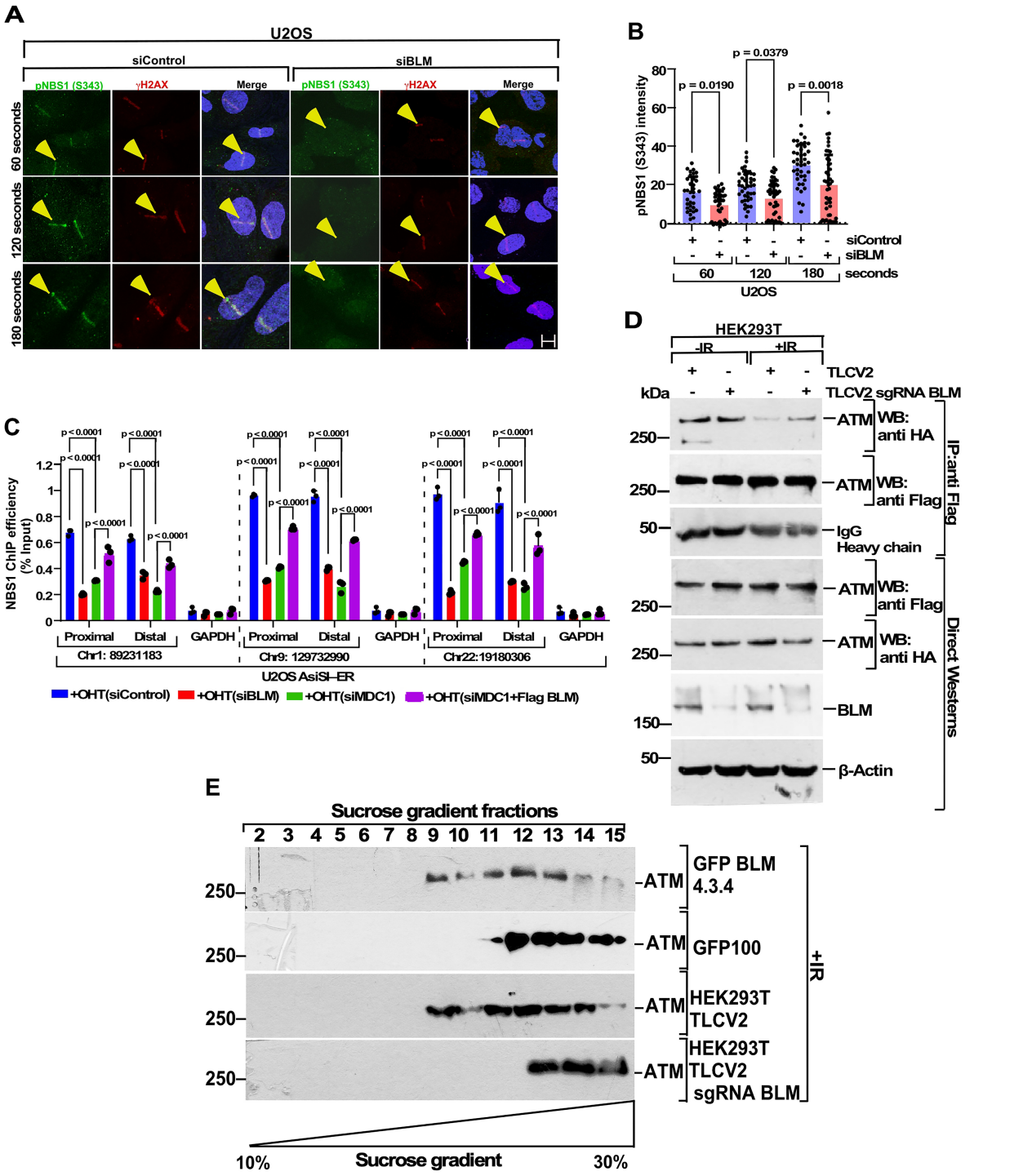

Figure 3. Presence of BLM enhances ATM monomerization. (A, B) BLM regulates the early recruitment of pNBS1 and γH2AX at laser microirradiation stripes. Laser microirradiation was performed on U2OS cells after transfecting them with either siControl or siBLM. Cells were fixed 60, 120, and 180 s post-laser microirradiation. (**A**) Immunostaining was carried out using anti-pNBS1 (S343) and γH2AX antibodies. The nuclei were stained with DAPI. Bar: 2 μM. (**B**) Quantitation of pNBS1 (S343). Quantitation was done from 21 stripes obtained from three independent experiments (mean ± SD). (**C**) BLM promotes NBS1 recruitment at AsiSI-induced DSBs. U2OS-AsiSI-ER cells were transfected with either siControl, siBLM, or siMDC1 siRNA or siMDC1 cells transfected with Flag BLM. Forty-eight hours post-transfection, the cells were treated with 4-OHT for 30 min. ChIP was carried out using an anti-NBS1 antibody using chromatin obtained from these cells. NBS1 recruitment to the three AsiSI-induced DSBs or GAPDH loci was determined by ChIP-qPCR. Data are from three independent experiments (mean ± SD). (**D**) Presence of BLM promotes ATM monomerization after IR exposure. Flag-tagged ATM and HA-tagged ATM were cotransfected in HEK293T TLCV2 and HEK293T TLCV2 sgRNA BLM cells for 36 h. Cells were exposed to 3 Gy IR. One hour post-IR, lysates were prepared. Immunoprecipitation was carried out with anti-Flag beads and co-immunoprecipitated proteins detected using the indicated antibodies (top). (Bottom) Direct westerns of the lysates used for immunoprecipitation. The experiment was repeated three times. (**E**) Presence of BLM potentiates ATM monomerization. Whole-cell lysates were prepared from two isogenic pairs of cells—GFP-BLM Clone 4.3.4/GFP-100 and HEK293T TLCV2/HEK293T TLCV2 sgRNA BLM after exposing the cells to IR (3 Gy). Lysates (prepared 60 min post-IR) were separated through a 10%–30% continuous sucrose gradient via ultracentrifugation, after which the fractions were collected from top to bottom and analyzed by immunoblot using anti-ATM antibody. The experiment was repeated three times.

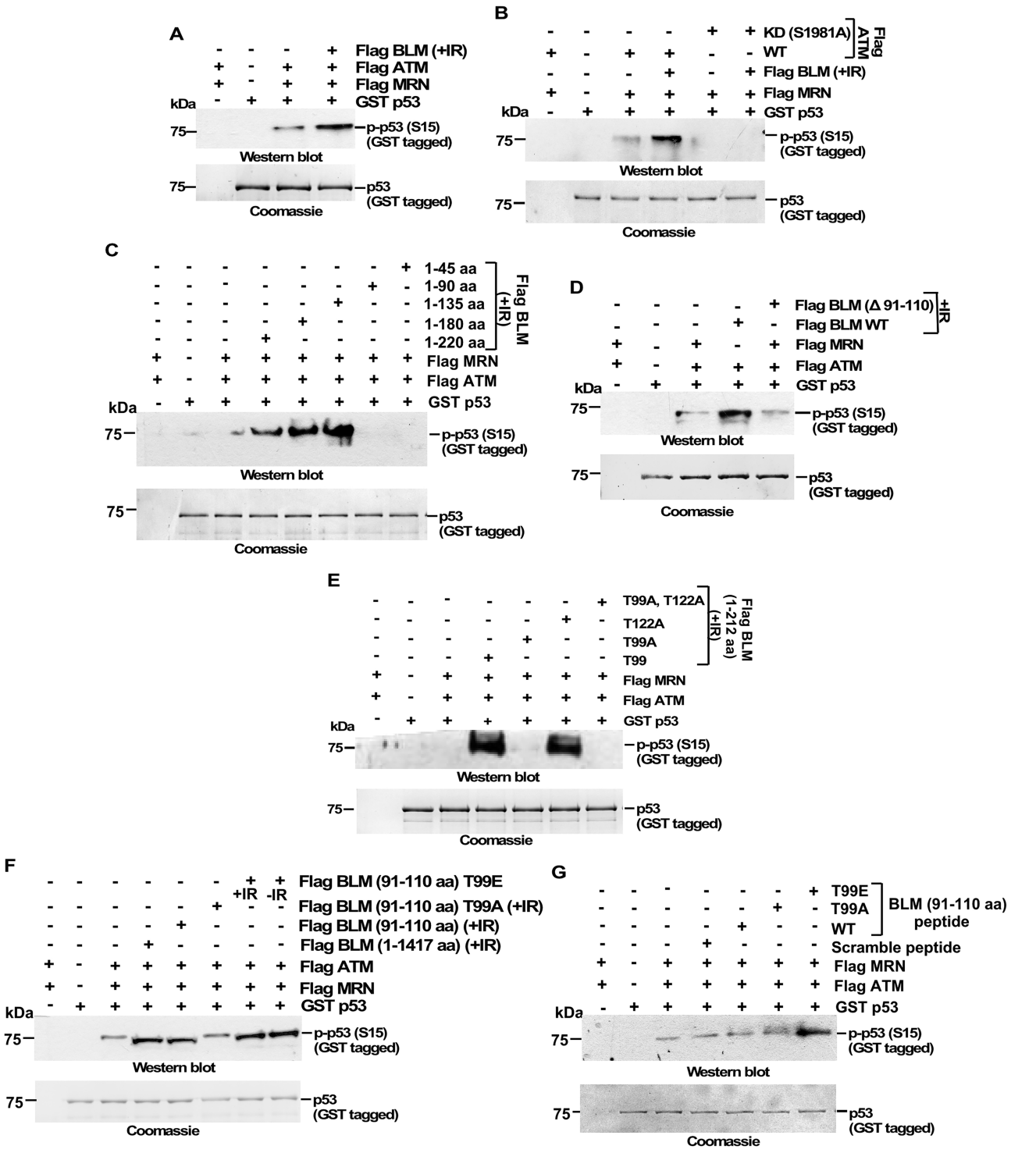

Figure 4. BLM enhances ATM kinase activity. (**A**) Immunopurified BLM from cells exposed to IR enhances ATM kinase activity. *In vitro* ATM kinase assay was carried out in the presence of Flag BLM immunopurified from HEK293T cells 1 h after exposure to 3 Gy IR, immunopurified Flag ATM and Flag MRN complex from HEK293T cells not exposed to IR, GST p53, and linear ssDNA. ATM kinase activity was determined by the phosphorylation of p53 using an antibody against p53 (S15). GST p53 Coomassie shows an equal amount of p53 in all the reactions. The experiment was repeated three times. (**B**) BLM enhances the kinase activity of only wild-type ATM. Same as panel (A), except ATM kinase was carried out with either Flag ATM wild-type or Flag ATM (S1981A). The experiment was repeated three times. (**C**) BLM (1–135 aa) enhances ATM kinase activity. Same as panel (A), except ATM kinase was set up with immunopurified Flag BLM (1–45 aa), Flag BLM (1–90 aa), Flag BLM (1–135 aa), Flag BLM (1–180 aa), and Flag BLM (1–220 aa). The experiment was repeated three times. (**D**) BLM (91–110 aa) is essential for the enhancement of ATM kinase activity. Same as panel (A), except ATM kinase assay was set up with immunopurified Flag BLM WT and Flag BLM (Δ91–110). The experiment was repeated three times. (**E**) Phosphorylation of BLM at Thr99 is essential to enhance ATM kinase activity. Same as panel (A), except ATM kinase assay was set up with immunopurified Flag BLM (1–212) T99, Flag BLM (1–212) T99A, Flag BLM (1–212) T122A, and Flag BLM (1–212) T99A, T122A. The experiment was repeated three times. (F, G) BLM (91–110) T99E peptide constitutively enhances ATM kinase activity. ATM kinase was set up with (**F**) immunopurified Flag BLM (1–1417), Flag BLM (91–110), Flag BLM (91–110) T99A, and Flag BLM (91–110) T99E peptides or (**G**) synthesized peptides corresponding to a scrambled sequence, BLM (91–110) wild-type sequence, BLM (91–110) T99A, and BLM (91–110) T99E were used in the kinase assays. Both experiments were repeated three times.

enhancing p53 phosphorylation lies between amino acids 91 and 110 (Fig. 4C and D; summarized in Supplementary Fig. S5C).

It is known that upon DNA damage, ATM interacts with BLM and directly phosphorylates BLM on Thr99 and Thr122 [9]. We wanted to know whether the presence of BLM phosphorylated at Thr99/Thr122 was essential for the ability of BLM to enhance ATM phosphorylation. We found that BLM phosphorylated at Thr99, but not Thr122 was essential to enhance ATM-mediated phosphorylation on p53 by ∼4.3-fold (Fig. 4E). Further immunopurified Flag BLM (91–110) and phosphomimetic Flag BLM (91–110) T99E but not phospho-dead Flag BLM (91–110) T99A from cells exposed to IR enhanced ATM-mediated p53 Ser15 phosphorylation. In fact, the phosphomimetic Flag BLM (91–110) T99E could enhance the phosphorylation by almost 2.6-fold when it was isolated from asynchronously growing cells (i.e. not exposed to IR) (Fig. 4F). Exogenous addition of synthetic BLM (91–110) T99E peptide also enhanced ATM-mediated p53 phosphorylation by 2.3-fold (Fig. 4G). Human-derived BLM (91–110) also enhanced murine ATM-mediated phosphorylation of p53 by ∼2.6-fold (Supplementary Fig. S5D).

The N-terminal region of BLM (1–294) has been reported to exhibit single-strand annealing and strand exchange activity [27]. However, all three variants of BLM displayed a similar level of strand annealing activity, indicating that this activity is independent of BLM's phosphorylation status at Thr99 (Supplementary Fig. S5E).

BLM (91–110) acts as an agonist of DDR response

Based on the above results, we wanted to understand whether the expression of BLM (91–110) is enough to disrupt ATM dimerization. For this purpose, incubation of the ATM dimer (consisting of HA-ATM and Bio-Flag-ATM) with purified MRN complex and the different synthetic BLM (91–110) peptides showed the maximum presence of HA-ATM in the supernatant in case of the phosphomimetic BLM (91–110) T99E peptide by ∼3.4-fold (Supplementary Fig. S6A), indicating that phosphorylated BLM (91–110) can disrupt ATM dimer. To recapitulate this ability *in vivo*, HEK293T sgRNA BLM cells were cotransfected with Flag-ATM and HA-ATM in the presence of constructs expressing His-tagged BLM (91–110) variants in the presence or absence of IR exposure. Immunoprecipitation with anti-Flag antibody revealed enhanced interaction (by ∼1.6-fold) between Flag-ATM and HA-ATM either in the absence of BLM or in cells expressing phospho-dead His BLM (91–110) T99A, indicating that only under these conditions ATM dimer is not dissociated (Fig. 5A). Reciprocally, this also demonstrated that BLM (91–110), phosphorylated at Thr99 (either due to IR or constitutively as in the case of T99E phosphomimetic), is capable of disrupting the ATM dimer (Fig. 5A). Mechanistically, this occurs because all BLM (91–110) variants, except the phospho-dead T99A, can interact with endogenous NBS1 after IR exposure (Fig. 5B). Reciprocally, a deletion mutant not expressing BLM (91–110) interacts minimally with endogenous NBS1 (Fig. 5C). Interestingly, while ATM interacts with NBS1, BLM (91–110) did not directly interact with the kinase, both *in vivo* and *in vitro* (Fig. 5B and Supplementary Fig. S6B). Previously, we have demonstrated that BLM undergoes ubiquitination at lysine residues K105, K225, and K259. The polyubiquitylated BLM served as a critical factor for its interaction with NBS1 [22, 28]. We now investigated whether phosphorylation of BLM at Thr99 affected its N-terminal ubiquitylation and how the ubiquitylated cum phosphorylated BLM interacted with NBS1 after DNA damage. We found that ubiquitination of BLM was maximum for BLM (1–1417) T99E (enhanced by 3.2-fold), which in turn leads to its increased interaction with NBS1 (by 1.4-fold) (Fig. 5D).

In an effort to understand whether BLM (91–110) can be utilized as a DDR agonist, we generated four stable lines via lentiviral transduction in hTERT immortalized BS fibroblast, BS3509, by expressing Flag BLM (91–110), Flag BLM (91–110) T99A, Flag BLM (91–110) T99E, and Flag BLM 1–1417 (Δ91–110) (Supplementary Fig. S6C). After IR, the basal levels of pATM (S1981) (by 2.3-fold), p-p53 (S15) (by 2-fold), pMDC1 (T4) (by 1.7-fold), and γH2AX (by 2-fold) in BS3509 were all enhanced in cells expressing Flag BLM (91–110) and Flag BLM (91–110) T99E but not in cells expressing Flag BLM (91–110) T99A or Flag BLM 1–1417 (Δ91–110) [61] (Fig. 5E–H and Supplementary Fig. S6D and E). Interestingly, constitutive expression of BLM (91–110) T99E caused enhanced phosphorylation of ATM and its targets to a similar extent, even in the absence of exposing the cells to IR (Fig. 5E–H and Supplementary Fig. S6D and E), thereby indicating that BLM (91–110) peptide has the potential to function as a DDR agonist *in vivo*. We also investigated whether this effect is due to the inability of the BLM variants to exit Promyelocytic Leukemia (PML) nuclear bodies upon DNA damage. However, none of the cell lines, expressing BLM (1–1417), BLM (1–1417) T99A, and BLM (1–1417) T99E (Supplementary Fig. S6F), showed BLM–PML colocalization (Supplementary Fig. S6G). This indicates that the effectiveness of BLM WT and phosphomimetic BLM T99E (and the lack of effectiveness of the phospho-dead BLM T99A) to enhance the DDR was not due to the inability of BLM WT, T99A, or T99E to exit PML nuclear bodies after IR exposure.

Finally, we wanted to determine whether it is possible to use BLM (91–110) peptide to rescue the lack of ATM activation in BLM KO mice (as observed in Fig. 1G and H). Hence, BLM (91–110) T99A or T99E peptide was orthotopically injected into BLM KO mouse mammary tissue. After 9 days of injection, mice were either exposed or not exposed to 3 Gy IR. The mice were euthanized 1 h post-exposure and stained for pATM (S1981). A robust 2.6-fold autophosphorylation of ATM was observed in mouse mammary tissues injected with BLM (91–110) T99E peptide, regardless of whether the animals were exposed to IR or not. Critically, pATM (S1981) staining was not observed when BLM (91–110) T99A peptide was implanted in the mammary tissues (Fig. 5I and J). Together, the results indicate that BLM (91–110) peptide phosphorylated at Thr99 can act as a DDR agonist, thereby augmenting the pathway of DNA damage sensing, response, and finally repair.

Discussion

DDR is a complex signaling network essential for maintaining genomic integrity [33]. Multiple mechanisms have been proposed to activate ATM under different pathological and physiological conditions [34]. However, the major mechanism of activation of ATM by DSBs primarily occurs through the MRN complex [4]. NBS1 is known to directly bind to ATM dimers via its FxF/Y motif, disrupting the inactive ATM dimers into active monomers [39]. Phosphorylated NBS1

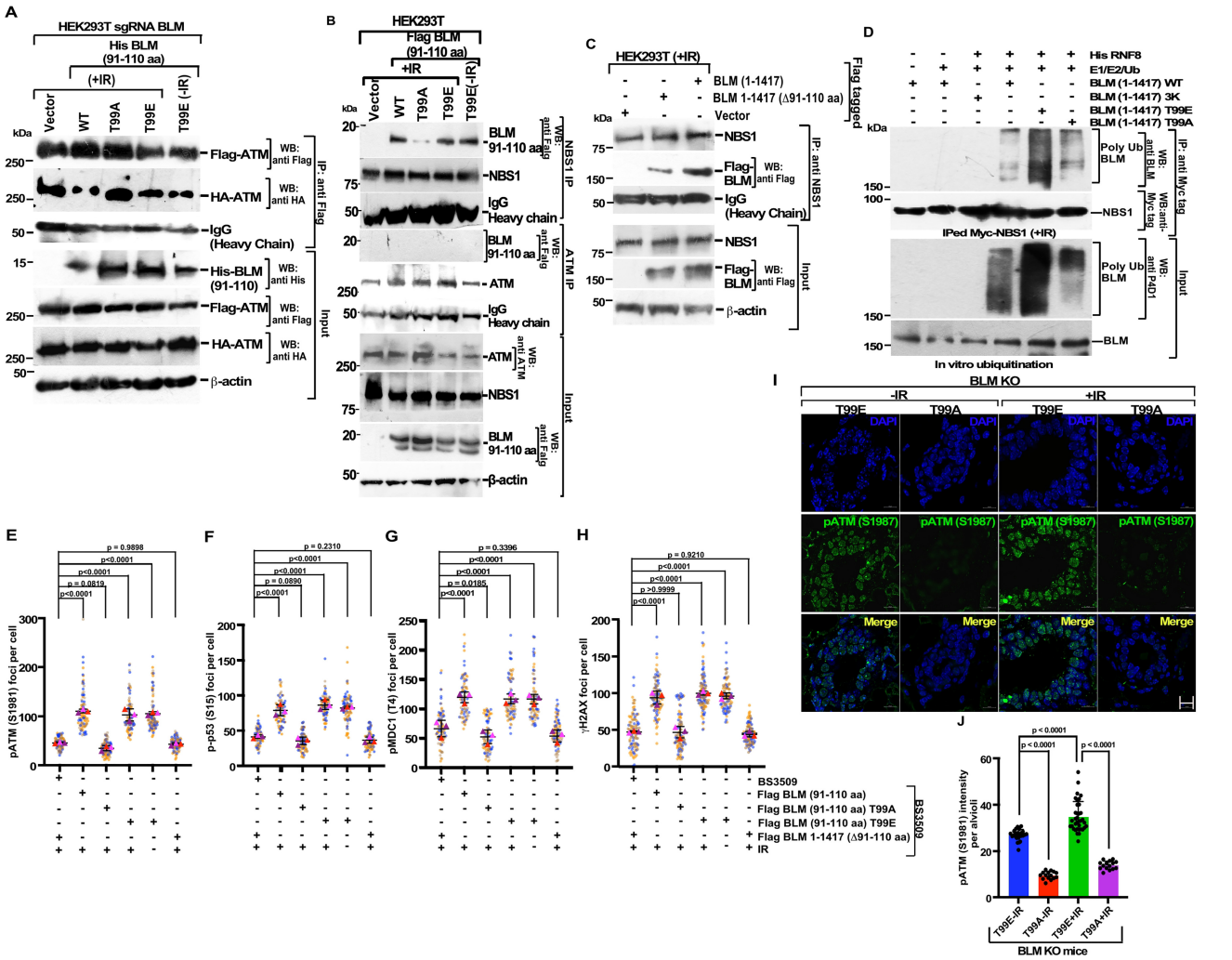

Figure 5. BLM (91–110 aa) T99E enhances DDR response. (**A**) ATM monomerization is enhanced in the presence of wild-type and T99E BLM (91–110 aa). His-tagged BLM (91–110 aa) wild-type (WT), BLM (91–110 aa) T99A, or BLM (91–110 aa) T99E, Flag-tagged ATM, and HA-tagged ATM were cotransfected in HEK293T TLCV2 sgRNA BLM cells for 36 h. Cells were either grown asynchronously or exposed to IR (3Gy). One hour post-IR, lysates were prepared. Immunoprecipitation was carried out with anti-Flag beads and co-immunoprecipitated proteins detected using anti-HA antibody (top). (Bottom) Direct westerns of the lysates used for immunoprecipitation. The experiment was repeated three times. (B, C) BLM (91–110 aa) interacts with NBS1 but not with ATM. Same as panel (A), except HEK293T cells were transfected with (**B**) Flag-tagged BLM (91–110 aa) wild-type (WT), BLM (91–110 aa) T99A, and BLM (91–110 aa) T99E or (**C**) BLM (1–1417 aa) and BLM 1–1417 (Δ91–110 aa). Cells were either grown asynchronously or exposed to IR (3 Gy). Immunoprecipitations were carried out with anti-NBS1 or anti-ATM antibodies, as indicated. The experiment was repeated three times. (**D**) Ubiquitylation of phosphorylated BLM enhances its interaction with NBS1. (Bottom, Input) *In vitro*, ubiquitylation reactions were carried out using full-length BLM (WT/T99E/T99A/3K ubiquitin mutant) using RNF8 as the E3 ligase. The ubiquitylated BLM was detected by an anti-P4D1 antibody. (Top, Interaction) Immunoprecipitated Myc-tagged NBS1 was obtained from HEK293T cells (grown in +IR condition). The interaction was carried out with bound Myc-tagged NBS1 and *in vitro* translated polyubiquitylated or nonubiquitylated BLM (from the bottom panel). BLM interacting with Nbs1 was detected with an anti-BLM antibody. (E–H) Flag BLM (91–110 aa) T99E increases the foci formation of DDR factors. Quantitation of immunofluorescence carried out in BS3509 cells or BS3509 cells stably expressing Flag-tagged BLM (91–110), BLM (91–110) T99A, BLM (91–110) T99E, or BLM 1–1417 (Δ91–110). The cells were either exposed to IR or grown asynchronously, as indicated. The antibodies used were against (**E**) pATM (S1981), (**F**) p-p53 (S15), (**G**) pMDC1 (T4), and (**H**) γH2AX. Quantitation was done from 90 cells obtained from three independent experiments (mean ± SD). The experiment was repeated three times and presented using SuperPlots [61]. (I, J) Lack of phosphorylated ATM in BLM KO mice is rescued upon injecting BLM (91–110 aa) T99E peptide. Synthetic BLM peptide (91–110 aa) T99E or BLM peptide (91–110 aa) T99A was injected orthotopically with hydrogel into mice mammary fat pads of 12-week-old BLM KO female mice. After 9 days of injection, mice were either exposed or not exposed to 3Gy IR. One hour post-irradiation, the mice were sacrificed, and the mammary tissues were excised. (**I**) Immunofluorescence was carried out using anti-pATM (S1981) antibody, which recognizes pATM (S1987) in mice. The nuclei were stained with DAPI. Images depict a typical alveolus. Bar: 5 μM. (**J**) Quantitation of the intensity of pATM (S1987) per alveolus of mammary tissue (mean ± SD). Tissues analyzed were from four mice.

interacts with monomeric ATM, allowing the kinase to target downstream targets in response to DSBs (see the Graphical abstract, top panel).

Though BLM helicase is more well known for its role in stalled replication [13], it has also been implicated in the DDR pathway in response to DSBs. BLM interacts with ATM [9], and both proteins and the MRN complex are members of the BASC supercomplex [8]. BLM is also phosphorylated by ATM at Thr99 [9]. BLM is an early responder to DSBs and accumulates at the break sites in a biphasic manner. After DSB generation, recruitment of ubiquitylated BLM is dependent on ATM activity, MRN complex, and RNF8 [28]. Here, we demonstrate a feedforward loop between BLM and ATM, where ATM phosphorylates BLM at Thr99. The phosphorylated BLM undergoes enhanced ubiquitination, promoting its binding to NBS1. This interaction facilitates more efficient disruption of the ATM dimer, leading to increased ATM activation (see the Graphical abstract, middle panel).

Regulation of MRN-dependent ATM activity depends on multiple components. It has been shown that conformation changes in the MRN complex regulate ATM activity [40]. Further homeodomain proteins directly bind to ATM and MRN and regulate the kinase activity [26]. Two E3 ligases, Skp2 and Pellino, also regulate ATM activation via NBS1 ubiquitylation [41, 42]. It is quite possible that BLM may act as the adaptor protein, which allows better ubiquitylation of Nbs1. Indeed, the role of BLM as an adaptor protein involved in enhancing ubiquitylation of E3 ligase substrates is known [43, 44].

The ability of BLM to enhance ATM monomerization is due to an internal stretch of 20 amino acids (91–110 aa). Within that stretch, Thr99 is known to be phosphorylated by ATM [9]. In fact, the phosphomimetic version of the 20-mer BLM peptide can independently enhance DDR in both cells and mouse mammary tissues, causing ATM activation without the need for any DSB. Although ATM kinase activation has previously been shown to occur independently of DNA damage sensors or DNA lesions [45, 46], no biological reagent or tool has yet been identified that can enhance the DDR on demand. The 20-mer phosphomimetic BLM peptide fulfills this lacuna and can serve as an agonist of the DDR pathway (see the Graphical abstract, bottom panel).

The question that can be asked is why we need a DDR agonist, especially when potent ATM inhibitors (like KU-55933) are being thought of as potential tools for cancer therapy [47, 48]. ATM inhibitors potentially act by increasing the sensitivity of cancer cells to chemotherapeutic drugs or IR. While the clinical potential of ATM inhibitors remains huge, none of the inhibitors has successfully crossed Phase I clinical trials to date due to a variety of factors (e.g. see [49]). In contrast, it has been recognized for a long time that DDR is the primary bulwark against neoplastic transformation [50, 51] It is proposed that the naturally occurring phosphomimetic BLM peptide can act as the barrier to neoplastic transformation by augmenting and/or reactivating the DDR response (both in the niche and in the precancerous mass), which would delay or can even prevent cancer initiation and thereby cancer progression. For example, the peptide can also be used to activate ATM in Myc-overexpressing tumors, thereby triggering the ATM-mediated p53 response to induce apoptosis and suppress tumorigenesis [52]. Loss of ATM can lead to cancer stemness, epithelial–mesenchymal transition in pancreatic ductal adenocarcinoma, and breast cancer [53, 54]. Low levels of ATM were observed in both malignant tumors and stromal tissue, which are believed to contribute to the development of aggressive breast carcinoma [55]. ATM-deficient mice and patients are predisposed to lymphoma, susceptible to various cancers, and experience premature aging along with impaired telomere maintenance [56, 57]. Reduced ATM levels result in impaired embryo development, decreased oocyte quality, accumulation of DSBs, and increased susceptibility to genotoxic stress, ultimately leading to cellular senescence [58]. In addition, numerous substitution mutations, including missense and silent coding mutations, have been identified within the BLM region spanning 91–110 aa in cancer patients (https://cancer.sanger.ac.uk/cosmic) [59]. However, the functional implications of these mutations remain unexplored. We propose that these mutations may contribute to the initiation of carcinogenesis by leading to the accumulation of damaged DNA and, consequently, causing genome instability. The phosphomimetic BLM peptide can be theoretically used in each of the above cases—boosting the ATM-mediated DDR and fully or partially reverting the effects, and can, therefore, be considered for usage for delaying and/or prevention of both cancer and aging.

Acknowledgements

The authors acknowledge Michael Kastan, Tanya Paull, Didier Trono, Adam Karpf, and Ian Hickson for plasmids, and Jerry Shay and Gaelle Legube for cells. The authors thank Shabih Fatema Rezvi and Divyasree Marripati for their technical assistance.

Author contributions: Conceptualization: SS, RA, HA. Methodology: RA, HA,CM, BC, VS, VT, NK, SP, NG and GDJ. Investigation: RA, HA, CM, BC, VS and VT. Visualization: RA, HA, CM, BC, and VS. Data curation: RA and GDJ (Phosphoproteomics). Formal analysis: RA and HA. Resources: SS and AB (Hydrogel). Funding acquisition, Supervision: SS. Writing—original draft: RA and SS. Writing—review and editing: RA and SS.

Supplementary data

Supplementary data is available at NAR online.

Conflict of interest

None declared. Indian Patent Application No. 202431105277 has been filed based on this work.

Funding

The authors acknowledge funding from National Institute of Immunology and National Institute of Biomedical Genomics core funds (S.S.), Department of Biotechnology, Ministry of Science and Technology, India grant BT/PR41739/BRB/10/1974/2021 (S.S.), Board of Research in Nuclear Sciences, India grant 58/14/17/2021-BRNS (S.S.), Anusandhan National Research Foundation (ANRF)/Science and Engineering Research Board (SERB), India grant CRG/2020/000125 (S.S.), Council of Scientific and Industrial Research (CSIR), India grant 27/0387/23/EMR-II (S.S.), Indo-French Centre for the Promotion of Advanced Research (IFCPAR/CEFIPRA) grant IFC/6803-1/2022 (S.S.), and Anusandhan National Research Foundation (ANRF), India J.C. Bose Fellowship (JBR/2023/000020).

Data availability

The MS proteomics data have been deposited to the ProteomeXchange Consortium via the PRIDE [60] partner repository with the dataset identifier PXD048117.

References

1. Marechal A, Zou L. DNA damage sensing by the ATM and ATR kinases. *Cold Spring Harb Perspect Biol* 2013;**5**:a012716. https://doi.org/10.1101/cshperspect.a012716
2. Lee JH, Paull TT. Cellular functions of the protein kinase ATM and their relevance to human disease. *Nat Rev Mol Cell Biol* 2021;**22**:796–814. https://doi.org/10.1038/s41580-021-00394-2
3. Bakkenist CJ, Kastan MB. DNA damage activates ATM through intermolecular autophosphorylation and dimer dissociation. *Nature* 2003;**421**:499–506. https://doi.org/10.1038/nature01368
4. Lee JH, Paull TT. ATM activation by DNA double-strand breaks through the Mre11–Rad50–Nbs1 complex. *Science* 2005;**308**:551–4. https://doi.org/10.1126/science.1108297
5. Uziel T, Lerenthal Y, Moyal L *et al.* Requirement of the MRN complex for ATM activation by DNA damage. *EMBO J* 2003;**22**:5612–21. https://doi.org/10.1093/emboj/cdg541
6. Zhou Y, Lee JH, Jiang W *et al.* Regulation of the DNA damage response by DNA-PKcs inhibitory phosphorylation of ATM. *Mol Cell* 2017;**65**:91–104. https://doi.org/10.1016/j.molcel.2016.11.004
7. Lavin MF, Yeo AJ. Clinical potential of ATM inhibitors. *Mutat Res* 2020;**821**:111695. https://doi.org/10.1016/j.mrfmmm.2020.111695
8. Wang Y, Cortez D, Yazdi P *et al.* BASC, a super complex of BRCA1-associated proteins involved in the recognition and repair of aberrant DNA structures. *Genes Dev* 2000;**14**:927–39. https://doi.org/10.1101/gad.14.8.927
9. Beamish H, Kedar P, Kaneko H *et al.* Functional link between BLM defective in Bloom's syndrome and the ataxia-telangiectasia-mutated protein, ATM. *J Biol Chem* 2002;**277**:30515–23. https://doi.org/10.1074/jbc.M203801200
10. Payne M, Hickson ID. Genomic instability and cancer: lessons from analysis of Bloom's syndrome. *Biochem Soc Trans* 2009;**37**:553–9. https://doi.org/10.1042/BST0370553
11. Kaur E, Agrawal R, Arun R *et al.* Small molecules that disrupt RAD54–BLM interaction hamper tumor proliferation in colon cancer chemoresistance models. *J Clin Invest* 2024;**134**:e161941. https://doi.org/10.1172/JCI161941
12. Srivastava V, Modi P, Tripathi V *et al.* BLM helicase stimulates the ATPase and chromatin-remodeling activities of RAD54. *J Cell Sci* 2009;**122**:3093–103. https://doi.org/10.1242/jcs.051813
13. Kaur E, Agrawal R, Sengupta S. Functions of BLM helicase in cells: is it acting like a double-edged sword? *Front Genet* 2021;**12**:634789. https://doi.org/10.3389/fgene.2021.634789
14. Tikoo S, Sengupta S. Time to bloom. *Genome Integr* 2010;**1**:14. https://doi.org/10.1186/2041-9414-1-14
15. Tripathi V, Nagarjuna T, Sengupta S. BLM helicase-dependent and -independent roles of 53BP1 during replication stress-mediated homologous recombination. *J Cell Biol* 2007;**178**:9–14. https://doi.org/10.1083/jcb.200610051
16. Bugreev DV, Yu X, Egelman EH *et al.* Novel pro- and anti-recombination activities of the Bloom's syndrome helicase. *Genes Dev* 2007;**21**:3085–94. https://doi.org/10.1101/gad.1609007
17. Nimonkar AV, Genschel J, Kinoshita E *et al.* BLM–DNA2–RPA–MRN and EXO1–BLM–RPA–MRN constitute two DNA end resection machineries for human DNA break repair. *Genes Dev* 2011;**25**:350–62. https://doi.org/10.1101/gad.2003811
18. Grabarz A, Guirouilh-Barbat J, Barascu A *et al.* A role for BLM in double-strand break repair pathway choice: prevention of CtIP/Mre11-mediated alternative nonhomologous end-joining. *Cell Rep* 2013;**5**:21–8. https://doi.org/10.1016/j.celrep.2013.08.034
19. Sengupta S, Robles AI, Linke SP *et al.* Functional interaction between BLM helicase and 53BP1 in a Chk1-mediated pathway during S-phase arrest. *J Cell Biol* 2004;**166**:801–13. https://doi.org/10.1083/jcb.200405128
20. Tripathi V, Kaur S, Sengupta S. Phosphorylation-dependent interactions of BLM and 53BP1 are required for their anti-recombinogenic roles during homologous recombination. *Carcinogenesis* 2008;**29**:52–61. https://doi.org/10.1093/carcin/bgm238
21. Davies SL, North PS, Dart A *et al.* Phosphorylation of the Bloom's syndrome helicase and its role in recovery from S-phase arrest. *Mol Cell Biol* 2004;**24**:1279–91. https://doi.org/10.1128/MCB.24.3.1279-1291.2004
22. Tikoo S, Madhavan V, Hussain M *et al.* Ubiquitin-dependent recruitment of the Bloom syndrome helicase upon replication stress is required to suppress homologous recombination. *EMBO J* 2013;**32**:1778–92. https://doi.org/10.1038/emboj.2013.117
23. Kaur S, Modi P, Srivastava V *et al.* Chk1-dependent constitutive phosphorylation of BLM helicase at serine 646 decreases after DNA damage. *Mol Cancer Res* 2010;**8**:1234–47. https://doi.org/10.1158/1541-7786.MCR-10-0233
24. Guiley KZ, Iness AN, Saini S *et al.* Structural mechanism of Myb–MuvB assembly. *Proc Natl Acad Sci USA* 2018;**115**:10016–21. https://doi.org/10.1073/pnas.1808136115
25. Pal S, Medatwal N, Kumar S *et al.* A localized chimeric hydrogel therapy combats tumor progression through alteration of sphingolipid metabolism. *ACS Cent Sci* 2019;**5**:1648–62. https://doi.org/10.1021/acscentsci.9b00551
26. Johnson TE, Lee JH, Myler LR *et al.* Homeodomain proteins directly regulate ATM kinase activity. *Cell Rep* 2018;**24**:1471–83. https://doi.org/10.1016/j.celrep.2018.06.089
27. Chen CF, Brill SJ. An essential DNA strand-exchange activity is conserved in the divergent N-termini of BLM orthologs. *EMBO J* 2010;**29**:1713–25. https://doi.org/10.1038/emboj.2010.61
28. Tripathi V, Agarwal H, Priya S *et al.* MRN complex-dependent recruitment of ubiquitylated BLM helicase to DSBs negatively regulates DNA repair pathways. *Nat Commun* 2018;**9**:1016. https://doi.org/10.1038/s41467-018-03393-8
29. Day M, Oliver AW, Pearl LH. Phosphorylation-dependent assembly of DNA damage response systems and the central roles of TOPBP1. *DNA Repair (Amst)* 2021;**108**:103232. https://doi.org/10.1016/j.dnarep.2021.103232
30. Lanz MC, Dibitetto D, Smolka MB. DNA damage kinase signaling: checkpoint and repair at 30 years. *EMBO J* 2019;**38**:e101801. https://doi.org/10.15252/embj.2019101801
31. Slenter DN, Kutmon M, Hanspers K *et al.* WikiPathways: a multifaceted pathway database bridging metabolomics to other omics research. *Nucleic Acids Res* 2018;**46**:D661–7. https://doi.org/10.1093/nar/gkx1064
32. Barrett T, Wilhite SE, Ledoux P *et al.* NCBI GEO: archive for functional genomics data sets—update. *Nucleic Acids Res* 2013;**41**:D991–5. https://doi.org/10.1093/nar/gks1193
33. Ciccia A, Elledge SJ. The DNA damage response: making it safe to play with knives. *Mol Cell* 2010;**40**:179–204. https://doi.org/10.1016/j.molcel.2010.09.019
34. Paull TT. Mechanisms of ATM activation. *Annu Rev Biochem* 2015;**84**:711–38. https://doi.org/10.1146/annurev-biochem-060614-034335
35. Lou Z, Minter-Dykhouse K, Franco S *et al.* MDC1 maintains genomic stability by participating in the amplification of ATM-dependent DNA damage signals. *Mol Cell* 2006;**21**:187–200. https://doi.org/10.1016/j.molcel.2005.11.025
36. Chapman JR, Jackson SP. Phospho-dependent interactions between NBS1 and MDC1 mediate chromatin retention of the MRN complex at sites of DNA damage. *EMBO Rep* 2008;**9**:795–801. https://doi.org/10.1038/embor.2008.103

37. Melander F, Bekker-Jensen S, Falck J *et al.* Phosphorylation of SDT repeats in the MDC1 N terminus triggers retention of NBS1 at the DNA damage-modified chromatin. *J Cell Biol* 2008;**181**:213–26. https://doi.org/10.1083/jcb.200708210
38. Spycher C, Miller ES, Townsend K *et al.* Constitutive phosphorylation of MDC1 physically links the MRE11–RAD50–NBS1 complex to damaged chromatin. *J Cell Biol* 2008;**181**:227–40. https://doi.org/10.1083/jcb.200709008
39. Warren C, Pavletich NP. Structure of the human ATM kinase and mechanism of Nbs1 binding. *eLife* 2022;**11**:e74218. https://doi.org/10.7554/eLife.74218
40. Lee JH, Mand MR, Deshpande RA *et al.* Ataxia telangiectasia-mutated (ATM) kinase activity is regulated by ATP-driven conformational changes in the Mre11/Rad50/Nbs1 (MRN) complex. *J Biol Chem* 2013;**288**:12840–51. https://doi.org/10.1074/jbc.M113.460378
41. Ha GH, Ji JH, Chae S *et al.* Pellino1 regulates reversible ATM activation via NBS1 ubiquitination at DNA double-strand breaks. *Nat Commun* 2019;**10**:1577. https://doi.org/10.1038/s41467-019-09641-9
42. Wu J, Zhang X, Zhang L *et al.* Skp2 E3 ligase integrates ATM activation and homologous recombination repair by ubiquitinating NBS1. *Mol Cell* 2012;**46**:351–61. https://doi.org/10.1016/j.molcel.2012.02.018
43. Chandra S, Priyadarshini R, Madhavan V *et al.* Enhancement of c-Myc degradation by BLM helicase leads to delayed tumor initiation. *J Cell Sci* 2013;**126**:3782–95.
44. Priyadarshini R, Hussain M, Attri P *et al.* BLM potentiates c-Jun degradation and alters its function as an oncogenic transcription factor. *Cell Rep* 2018;**24**:947–61. https://doi.org/10.1016/j.celrep.2018.06.101
45. Soutoglou E, Misteli T. Activation of the cellular DNA damage response in the absence of DNA lesions. *Science* 2008;**320**:1507–10. https://doi.org/10.1126/science.1159051
46. Hartlerode AJ, Morgan MJ, Wu Y *et al.* Recruitment and activation of the ATM kinase in the absence of DNA-damage sensors. *Nat Struct Mol Biol* 2015;**22**:736–43. https://doi.org/10.1038/nsmb.3072
47. Hickson I, Zhao Y, Richardson CJ *et al.* Identification and characterization of a novel and specific inhibitor of the ataxia-telangiectasia mutated kinase ATM. *Cancer Res* 2004;**64**:9152–9. https://doi.org/10.1158/0008-5472.CAN-04-2727
48. Stakyte K, Rotheneder M, Lammens K *et al.* Molecular basis of human ATM kinase inhibition. *Nat Struct Mol Biol* 2021;**28**:789–98. https://doi.org/10.1038/s41594-021-00654-x
49. Waqar SN, Robinson C, Olszanski AJ *et al.* Phase I trial of ATM inhibitor M3541 in combination with palliative radiotherapy in patients with solid tumors. *Invest New Drugs* 2022;**40**:596–605. https://doi.org/10.1007/s10637-022-01216-8
50. Bartkova J, Horejsi Z, Koed K *et al.* DNA damage response as a candidate anti-cancer barrier in early human tumorigenesis. *Nature* 2005;**434**:864–70. https://doi.org/10.1038/nature03482
51. Gorgoulis VG, Vassiliou LV, Karakaidos P *et al.* Activation of the DNA damage checkpoint and genomic instability in human precancerous lesions. *Nature* 2005;**434**:907–13. https://doi.org/10.1038/nature03485
52. Pusapati RV, Rounbehler RJ, Hong S *et al.* ATM promotes apoptosis and suppresses tumorigenesis in response to Myc. *Proc Natl Acad Sci USA* 2006;**103**:1446–51. https://doi.org/10.1073/pnas.0507367103
53. Russell R, Perkhofer L, Liebau S *et al.* Loss of ATM accelerates pancreatic cancer formation and epithelial–mesenchymal transition. *Nat Commun* 2015;**6**:7677. https://doi.org/10.1038/ncomms8677
54. Drosos Y, Escobar D, Chiang MY *et al.* ATM-deficiency increases genomic instability and metastatic potential in a mouse model of pancreatic cancer. *Sci Rep* 2017;**7**:11144. https://doi.org/10.1038/s41598-017-11661-8
55. Feng X, Li H, Dean M *et al.* Low ATM protein expression in malignant tumor as well as cancer-associated stroma are independent prognostic factors in a retrospective study of early-stage hormone-negative breast cancer. *Breast Cancer Res* 2015;**17**:65. https://doi.org/10.1186/s13058-015-0575-2
56. Hande MP, Balajee AS, Tchirkov A *et al.* Extra-chromosomal telomeric DNA in cells from Atm(−/−) mice and patients with ataxia-telangiectasia. *Hum Mol Genet* 2001;**10**:519–28. https://doi.org/10.1093/hmg/10.5.519
57. Liyanage M, Weaver Z, Barlow C *et al.* Abnormal rearrangement within the alpha/delta T-cell receptor locus in lymphomas from Atm-deficient mice. *Blood* 2000;**96**:1940–6. https://doi.org/10.1182/blood.V96.5.1940
58. Suzuki R, Tan X, Szymanska KJ *et al.* The role of declining ataxia-telangiectasia-mutated (ATM) function in oocyte aging. *Cell Death Discov* 2024;**10**:302. https://doi.org/10.1038/s41420-024-02041-z
59. de Bruijn I, Kundra R, Mastrogiacomo B *et al.* Analysis and visualization of longitudinal genomic and clinical data from the AACR Project GENIE Biopharma Collaborative in cBioPortal. *Cancer Res* 2023;**83**:3861–7. https://doi.org/10.1158/0008-5472.CAN-23-0816
60. Perez-Riverol Y, Bai J, Bandla C *et al.* The PRIDE database resources in 2022: a hub for mass spectrometry-based proteomics evidences. *Nucleic Acids Res* 2022;**50**:D543–52. https://doi.org/10.1093/nar/gkab1038
61. Lord SJ, Velle KB, Mullins RD *et al.* SuperPlots: communicating reproducibility and variability in cell biology. *J Cell Biol* 2020;**219**:e202001064. https://doi.org/10.1083/jcb.202001064

Received: September 18, 2024. **Revised:** January 8, 2025. **Editorial Decision:** January 31, 2025. **Accepted:** February 5, 2025